Assessment of Beamforming Algorithms with Subarrayed Planar Arrays for B5G/6G LEO Non-Terrestrial Networks

M. Rabih Dakkak*, Daniel Gaetano Riviello*, Alessandro Guidotti†, Alessandro Vanelli-Coralli*
*Dept. of Electrical, Electronic, and Information Engineering (DEI), Univ. of Bologna, Bologna, Italy
†National Inter-University Consortium for Telecommunications (CNIT), Univ. of Bologna Research Unit, Italy
{mrabih.dakkak2, daniel.riviello, a.guidotti, alessandro.vanelli}@unibo.it

***Abstract*—Non-Terrestrial Networks (NTNs) in Beyond 5G (B5G) and 6G ecosystems are expected to play a crucial role in providing the requests of connections anywhere and anytime by offering wide-area coverage and ensuring service availability, continuity, and scalability. Full Frequency Reuse (FFR) schemes, which are able in cooperation with digital beamforming algorithms to cope with the substantial co-channel interference, are considered to be an efficient solution to meet the growing demand of high data rates in B5G/6G systems. In this paper, we propose a Limited Field Of View (LFOV) planar array architecture composed of smaller planar subarrays in order to increase the directivity of an on-board Low Earth Orbit (LEO) satellite antenna array and mitigate the interference. We evaluate the performance of feed-space beamforming schemes, including both full digital schemes based on Channel State Information (CSI) at the transmitter, such as Minimum Mean Square Error (MMSE), and full analog schemes that only require the users' locations, such as Conventional Beamforming (CBF). The numerical results of the system performance, presented by means of spectral efficiency, demonstrate a remarkable improvement in the proposed beamforming design with subarraying w.r.t. the one with no subarrayed configuration; in particular, we show that an analog beamforming scheme with subarraying can outperform a full digital beamforming scheme with no subarraying.**

***Index Terms*—6G, Non-Terrestrial Networks, MU-MIMO, beamforming, subarrays.**

I. Introduction and Motivation

Non-Terrestrial Networks (NTNs), integrated with Terrestrial Networks (TNs), are considered as a fundamental technology in Fifth Generation and beyond (B5G) mobile communication systems. This integration will facilitate global coverage for applications that require high resilience and high availability and, moreover, extend TN coverage to rural and under-served areas [1]. Such TN-NTN integration in 5G is envisaged in 3GPP Rel. 17 up to Rel.20 for 5G-Advanced [2].

To fulfill the high demands of B5G/6G systems, the academic and industrial communities have been concentrating on cutting-edge system-level strategies to boost the provided capacity by efficiently utilizing the available spectrum. One of these strategies is based on adding unused or underutilized spectrum portions in order to provide a flexible use of the spectrum such as Cognitive Radio solutions [3], and another approach is to consider full frequency reuse (FFR) in multi-beam satellite systems. Obviously, the second approach results in a significant amount of co-channel interference (CCI) from neighboring beams, requiring the adoption of high-level schemes to mitigate the interference, including precoding and beamforming [4]–[9] at the transmitting. As stated in [4]–[9], the implementation of beamforming schemes in NTNs has been comprehensively addressed for Geostationary Earth Orbit (GEO) systems and Low Earth Orbit (LEO) constellations. The main focus of these research studies concentrated on enhancing the data rate in unicast and/or multicast systems while also addressing the challenges associated with NTN-based beamforming, including scheduling algorithms and CSI recovery. Multi-User Multiple-Input Multiple-Output (MU-MIMO) is one of the most popular approaches utilized to meet the high demand of capacity. In this work [4], the authors provided a comprehensive survey on MIMO schemes implemented for SatCom, where the fixed and mobile SatCom systems are evaluated and the main channel impairments are addressed.

In [10] the authors provided an overview of the recent advances on antenna technology enabling the commercial applications of the planar arrays in SatCom. Although phased arrays have shown good advantages in terms of compactness, electronic steering, and fast reconfigurability with respect to traditional solutions (e.g., reflector antennas), there are still some issues such as the antenna affordability, its robustness, the Beamforming Network (BFN) complexity, the power efficiency and the increasing number of antenna elements needed to meet the growing demands of B5G systems. To proper address such complexity and cost issues, subarrayed configurations were introduced as one of the main solutions in [11]–[13], and has been implemented in MU-MIMO in [14]. In [8] the authors introduced a design of beamforming algorithms for MU-MIMO communications in LEO systems utilizing multiple subarrays, in which each radio frequency (RF) chain drives one subarray allowing the reduction in the number of beamforming ports and, consequently, relaxing the on-board processing requirements. Moreover, a novel beamforming architecture based on phased subarrays is proposed in [15] for TNs. This study showed that subarrays, when properly combined at the user locations, provide relatively high gains towards the intended users and sufficiently low inter-user interference levels. In [16], the authors introduced the architecture of Limited Field Of View (LFOV) arrays that

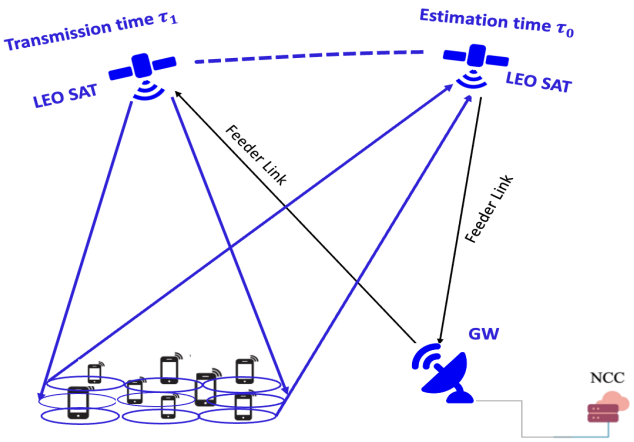

Fig. 1: LEO NTN system architecture.

use very narrow steering range, in which subarrays can be placed at a spacing larger than half of the wavelength to reduce the angular steering range and simultaneously increase the directivity withing the same range. When the spacing exceeds a value of half of the wavelength, the grating lobes issue is raised. However, they will appear outside the narrow steering range and thus will not impact performance in this type of application.

In this paper, we improve our LEO satellite system model in [17] through proposing a planar LFOV array architecture composed of smaller planar subarrays and we assess the performance of feed-space beamforming algorithms, in which the beamforming coefficients are computed only at subarray level, i.e., we assume that each subarray is controlled by a single RF-chain. The analyzed BF schemes are based on either: i) the CSI knowledge at the transmitter, i.e., digital Minimum Mean Square Error (MMSE) or ii) the users' location knowledge at the transmitter, i.e., analog Conventional Beamforming (CBF). Finally, as a further novelty, the satellite's movement is taken into account in this work. Fairness in the comparison between subarrayed and non subarrayed architectures is ensured by setting the same Effective Isotropic Radiated Power (EIRP) for all considered configurations.

A. Notation

In this paper, unless stated otherwise, the utilized notation is as follows: vectors are represented by bold lowercase letters and matrices by bold uppercase letters. The operator $(\cdot)^H$ refers to the matrix conjugate transposition. $\mathbf{A}_{i,:}$ and $\mathbf{A}_{:,i}$ refer the i-th row and the i-th column of matrix $\mathbf{A}$, respectively. Finally, tr$(\mathbf{A})$ denotes the trace of matrix $\mathbf{A}$.

II. System Model

We assume a single multi-beam LEO satellite at altitude $h_{sat} = 600$ km provided with an on-board planar antenna array of N_{tot} radiating elements organized into N subarrays, giving connection to K uniformly distributed on-ground UEs through S beams ($S < N$ and $S \ll K$). As stated earlier, FFR is supposed to be used, resulting in all beams utilizing identical spectral resources. To ensure the user connectivity, the LEO satellite shall establish a logical connection with a on-ground gNB. To achieve this, the satellite is presumed to be directly linked to a ground-based gateway (GW), as shown in Fig. 1. It is worth mentioning that the considered system model architecture is thoroughly described in [17]–[19]. The LEO satellite is supposed to enable digital beamforming schemes, which are detailed in the next section. These schemes require the estimates of either CSI or the users' locations, assumed to be performed by the UEs. As illustrated in Fig. 1, the estimates are calculated at a time instant τ_0, when the satellite is located at a specified position in its orbit. Afterwards, the estimates are returned to the network entity, i.e., the GW, to calculate the beamforming coefficients. Such coefficients are provided to the satellite for utilization within the BFN. Thus, as seen in Fig. 1, the actual beamformed transmission is performed at time instant $\tau_0 + \Delta\tau$. The time delay $\Delta\tau$ occurring between the phase of channel/location estimation and the phase of transmission causes a misalignment between the channel utilized for computing the beamforming matrix and the actual channel for transmission, thereby affecting the performance of the system. The delay is given as follows:

$$\Delta\tau = \tau_{ut,max} + 2\tau_{feeder} + \tau_p + \tau_{ad} \tag{1}$$

where: i) $\tau_{ut,max}$ is the maximum propagation delay for the UEs requesting connectivity in the coverage area; ii) τ_{feeder} is the delay on the feeder link, considered twice since the estimates need to be sent to the GW on the feeder downlink and then the beamformed symbols are returned on the feeder uplink to the satellite; iii) τ_p is the processing delay required to compute the beamforming coefficients; and iv) τ_{ad} defines any additional latency (e.g., large scale loss, scintillation, etc.). The antenna model and the array geometry are based on ITU-R Recommendation M.2101-0 [20]. Generally, the antenna boresight direction points to the Sub Satellite Point (SSP), while the point P represents the position of the user terminal on the ground. The user direction can be identified by the angle pair (ϑ, φ) where the boresight direction is (0,0). The direction cosines for the considered user can be expressed as: $u = \frac{P_y}{\|P\|}\sin\vartheta\sin\varphi$, and $v = \frac{P_z}{\|P\|}\cos\vartheta$. The overall array response of the Uniform Planar Array (UPA) made of subarrays in the direction (ϑ_i, φ_i) for user i can be expressed as the Kronecker product between the two array responses of the Uniform Linear Arrays (ULAs) lying on the y-axis and z-axis. Let us first define the $1 \times N_{\text{H}}$ Steering Vector (SV) of the ULA along the y-axis, $\mathbf{a}_{\text{H}}(\theta_i, \varphi_i)$, and the $1 \times N_{\text{V}}$ SV of the ULA along the z-axis, $\mathbf{a}_{\text{V}}(\theta_i)$ [21], [22]:

$$\mathbf{a}_{\text{H}}(\vartheta_i, \varphi_i) = \left[1, e^{jk_0 M_{\text{H}} d_{\text{H}} \sin\vartheta_i \sin\varphi_i}, \ldots, e^{jk_0 M_{\text{H}} d_{\text{H}} (N_{\text{H}}-1) \sin\vartheta_i \sin\varphi_i}\right] \tag{2}$$

$$\mathbf{a}_{\text{V}}(\vartheta_i) = \left[1, e^{jk_0 M_{\text{V}} d_{\text{V}} \cos\vartheta_i}, \ldots, e^{jk_0 M_{\text{V}} d_{\text{V}} (N_{\text{V}}-1) \cos\vartheta_i}\right] \tag{3}$$

where $k_0 = 2\pi/\lambda$ is the wave number, $N_{\text{H}}, N_{\text{V}}$ denote the number of subarrays on the horizontal and vertical directions, respectively, with $N = N_{\text{H}} N_{\text{V}}$, and $M_{\text{H}}, M_{\text{V}}$ denote the number

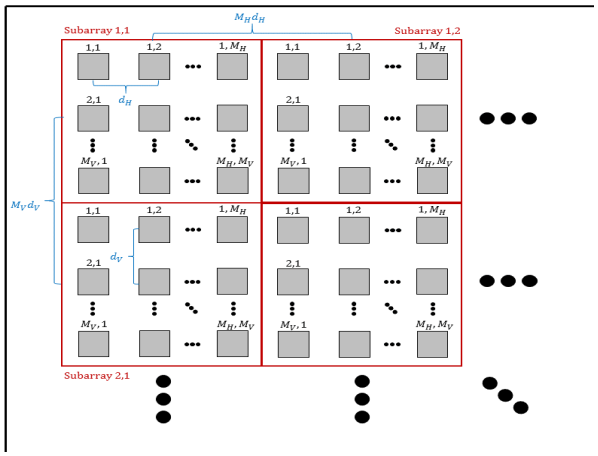

Fig. 2: Structure of the subarrayed UPA.

of antenna elements per each subarray on the horizontal (y-axis) and vertical (z-axis) directions, respectively, with $M = M_{\text{H}} M_{\text{V}}$, and finally $d_{\text{H}}, d_{\text{V}}$ denote the distance between adjacent antenna elements on the horizontal and vertical directions, respectively, as shown in Fig. 2. It is worth mentioning that the total number of antenna elements are $N_{tot} = MN$, where $M = 1$ if subarraying is not implemented. We can define the total steering vector of the full UPA (an array equipped with subarrays as antenna elements) as the Kronecker product of the 2 SV's along each axis:

$$\mathbf{a}_{\text{UPA}}(\vartheta_i, \varphi_i) = \mathbf{a}_{\text{H}}(\vartheta_i, \varphi_i) \otimes \mathbf{a}_{\text{V}}(\vartheta_i). \tag{4}$$

We further assume that the satellite is equipped with directive antenna elements, whose radiation pattern is denoted by $g_{\text{E}}(\vartheta_i, \varphi_i)$ according to Table 3 in [20], and these elements are grouped in N subarrays of size $M_{\text{H}} \times M_{\text{V}}$. It is worth recalling that a LFOV array has no steering nor beamforming capabilities at antenna element level, but only at subarray level; for this reason, the linear phase shifts of the SVs in (2) and (3) are taken w.r.t. the center of each subarray. We can define the subarray factor $F_{sub}(\vartheta_i, \varphi_i)$ as:

$$F_{sub}(\vartheta_i, \varphi_i) = \frac{\sin\left(\frac{M_{\text{V}}}{2} k_0 d_{\text{V}} \cos\vartheta_i\right)}{\sqrt{M_{\text{V}}} \sin\left(\frac{1}{2} k_0 d_{\text{V}} \cos\vartheta_i\right)} \frac{\sin\left(\frac{M_{\text{H}}}{2} k_0 d_{\text{H}} \sin\vartheta_i \sin\varphi_i\right)}{\sqrt{M_{\text{H}}} \sin\left(\frac{1}{2} k_0 d_{\text{H}} \sin\vartheta_i \sin\varphi_i\right)}. \tag{5}$$

Finally, we can express the total SV of the UPA of subarrays made of directive antenna elements at the satellite targeted for the i-th user as the product between the full UPA $\mathbf{a}_{\text{UPA}}(\vartheta_i, \varphi_i)$, the element radiation pattern, and the subarray factor:

$$\mathbf{a}(\vartheta_i, \varphi_i) = g_{\text{E}}(\vartheta_i, \varphi_i) F_{sub}(\vartheta_i, \varphi_i)\, \mathbf{a}_{\text{UPA}}(\vartheta_i, \varphi_i). \tag{6}$$

We adopt the same channel model and Key Performance Indicators (KPIs) described in [18], which we report here for the sake of clarity. The CSI vector, $\mathbf{h}_i$ represents the channel between the N radiating elements and the generic i-th on-ground UE, with $i = 1, ...K$, and can be written as:

$$\mathbf{h}_i = G_i^{(rx)} \frac{\lambda}{4\pi d_i} \sqrt{\frac{L_i}{\kappa B T_i}} e^{-j\frac{2\pi}{\lambda} d_i} \mathbf{a}(\vartheta_i, \varphi_i) \tag{7}$$

where: i) d_i is the slant range between the i-th user and the satellite,; ii) $\kappa B T_i$ refers to the equivalent thermal noise power, with κ being the Boltzmann's constant, B is the user bandwidth which is assumed to be the same for all users, and T_i is the equivalent noise temperature of the i-th user receiver; iii) L_i denotes the additional losses per user (e.g., atmospheric and antenna cable losses), and iv) $G_i^{(rx)}$ denotes the receiving antenna gain for the i-th UE. The additional losses are computed as $L_i = L_{sha,i} + L_{atm,i} + L_{sci,i}$, where $L_{sha,i}$ represents the log-normal shadow fading term, $L_{atm,i}$ the atmospheric loss, and $L_{sci,i}$ the scintillation, these terms are computed as per 3GPP TR 38.821 [23].

The system-level $K \times N$ complex channel matrix $\hat{\mathbf{H}}_{Sys}$ contains all of the K CSI vectors, where the generic i-th row denotes the CSI vector of the i-th user and the generic n-th column denotes the channel coefficients from the n-th on-board feed towards the K on-ground users. For each time slot, the Radio Resource Management (RRM) algorithm selects a subgroup of K_{sch} users to be scheduled, resulting in a $K_{sch} \times N$ complex scheduled channel matrix, $\hat{\mathbf{H}} = \mathcal{F}(\hat{\mathbf{H}}_{Sys})$ where $\mathcal{F}(\cdot)$ stands for the RRM function. Hence, $\hat{\mathbf{H}} \subseteq \hat{\mathbf{H}}_{Sys}$ is defined as a sub-matrix of $\hat{\mathbf{H}}_{Sys}$, which only includes the rows associated to the scheduled users. The proposed BF scheme calculates the $N \times K_{sch}$ complex beamforming matrix $\mathbf{W}$ which projects the K_{sch} dimensional column vector, $\mathbf{s} = [s_1, \ldots, s_{K_{sch}}]^T$, which contains the unit-variance user symbols, onto the N-dimensional space determined by the antenna feeds. The signal received by the i-th user could be expressed as [17]:

$$y_i = \underbrace{\mathbf{h}_i \mathbf{W}_{:,i}\, s_i}_{\text{intended}} + \underbrace{\sum_{k=1, k\neq i}^{K_{sch}} \mathbf{h}_i \mathbf{W}_{:,k}\, s_k}_{\text{interfering}} + z_i. \tag{8}$$

z_i denotes a circularly symmetric Gaussian random variable having zero mean and unit variance. The reason of unit variance is based on the observation that the channel coefficients given in (7) are normalized to the noise power. The K_{sch}-dimensional vector of received symbols is given as:

$$\mathbf{y} = \mathbf{H}_{\tau_1} \mathbf{W}_{\tau_0} \mathbf{s} + \mathbf{z}. \tag{9}$$

It is worth noting that, as already mentioned, the estimated channel matrix $\hat{\mathbf{H}}_{\tau_0}$, at time instant τ_0, is used to compute the beamforming coefficients, whereas, at time instant $\tau_1 = \tau_0 + \Delta\tau$, the utilized channel matrix is different and denoted as $\mathbf{H}_{\tau_1}$.

From (8), the Signal-to-Interference-plus-Noise Ratio (SINR) can be computed as:

$$\text{SINR}_i = \frac{||\mathbf{h}_i \mathbf{W}_{:,i}||^2}{1 + \sum_{k=1, k\neq i}^{K_{sch}} ||\mathbf{h}_i \mathbf{W}_{:,k}||^2}. \tag{10}$$

Given the above SINR expression, we can obtain the spectral efficiency associated to each user in a given time slot through

the Shannon bound formula or unconstrained capacity, which can be expressed as:

$$\eta_i = \log_2(1 + \text{SINR}_i). \tag{11}$$

III. Digital and analog beamforming schemes

The following analog/digital beamforming algorithms shall provide the benchmark for the evaluation performance:

a) Conventional Beamforming (CBF): It is also known as beam steering. In this approach, the weights are generated in order to produce a phase shift to compensate the delay of the direction (θ_i, φ_i) of the user of interest, and could be given by:

$$\mathbf{W}_{:,i} = \frac{1}{\sqrt{N}} \mathbf{a}^H_{\text{UPA}}(\vartheta_i, \varphi_i). \tag{12}$$

Since the weights are only made of complex exponentials with equal amplitude, it is a full analog beamforming scheme. CBF can be clearly considered as a location-based technique, since the direction (θ_i, φ_i) of the i-th user can be easily determined by knowing its location.

b) Minimum Mean Square Error (MMSE): It is considered the best full digital beamforming algorithm in the sense of SINR maximization; where the MMSE beamformer is realized to solve the MMSE problem as follows:

$$\mathbf{W}_{MMSE} = \arg\min_{\mathbf{W}} \text{E}||\hat{\mathbf{H}}\mathbf{W}\mathbf{s} + \mathbf{z} - \mathbf{s}||^2 \tag{13}$$

$$\mathbf{W}_{MMSE} = \hat{\mathbf{H}}^H(\hat{\mathbf{H}}\hat{\mathbf{H}}^H + \alpha \mathbf{I}_{K_{sch}})^{-1} \tag{14}$$

where $\hat{\mathbf{H}}$ is the estimated channel matrix, and α denotes the regularisation factor. Since the channel coefficients are normalised to the noise power, its optimal value is given by $\alpha = \frac{N}{P_t}$ [24], where P_t is the available transmitted power of the satellite.

Lastly, as explained in [7], the power normalization is a crucial aspect in beamforming as it ensures accurate consideration of the potential power output from both the satellite and each individual antenna. We contemplate two choices for power normalization of the MMSE beaforming matrix:

1) the Sum Power Constraint (SPC): an upper bound is imposed on the total on-board power as:

$$\tilde{\mathbf{W}} = \frac{\sqrt{P_t}\mathbf{W}}{\sqrt{\text{tr}(\mathbf{W}\mathbf{W}^H)}} \tag{15}$$

P_t being the the total power available on board maintains orthogonality among the beamformer columns, however, it cannot ensure an upper limit on the power transmitted from each feed. This implies the possibility of working in a non-linear regime.

2) Maximum Power Constraint (MPC) solution:

$$\tilde{\mathbf{W}} = \frac{\sqrt{P_t}\mathbf{W}}{\sqrt{N \max_j ||\mathbf{W}_{j,:}||^2}} \tag{16}$$

the power per antenna is upper bounded and the orthogonality is preserved, but not the entire available on-board power is exploited. Obviously, in case of CBF, SPC and MPC normalizations are equivalent since all matrix elements have equal amplitude.

TABLE I: System Configuration Parameters

Parameter	Value
Carrier frequency	S-band (2 GHz)
System band	30 MHz
Beamforming space	feed
Receiver type	fixed VSATs
Channel model	LOS
Propagation scenario	urban
Total on-board power density $P_{t,\text{dens}}$ without subarraying	4 dBW/MHz
Total on-board power density with subarraying	$P_{t,\text{dens}} - 10\log_{10}(M_\text{H}M_\text{V})$
Number of scheduled users K_{sch}	91
Number of subarrays N	1024 (32 $\times$32)
Number of elements per each subarray M	(2×2) (3×3), (4×4)
Number of antenna elements without subarraying $N_{tot} = N$	1024
Number of antenna elements with subarraying $N_{tot} = MN$	4096 9216, 16384
User density	0.5 user/km^2
Minimum elevation angle of the coverage area	76°
Angular scanning range $(\Delta\vartheta = \Delta\varphi)$	28°

IV. Numerical Assessment

We present the numerical results of the evaluation based on the parameters listed in Tab. I. The outcomes of the simulation are reported by means of Cumulative Distribution Functions (CDFs) of the spectral efficiency of the users. Assuming fixed positions of UEs, they are uniformly distributed with a density of 0.5 users/Km^2. This density translates to an average number of users $K = 28500$ to be served for each Monte Carlo iteration. The evaluation is carried out in full buffer condition, meaning that we assume unlimited traffic requirement.

Based on these premises, the users are scheduled based on their location. Specifically, a beam lattice is generated on ground only for scheduling purposes, as shown in Fig. 3, and a single user is randomly selected for each beam at each time slot; the total number of time slots is determined to ensure that every user is served at least once. Based on the coverage area shown in Fig. 3, it is possible to compute the minimum elevation angle, i.e., for a user at the edge of the coverage area, which is equal to 76°. This corresponds to a angular steering range for the array $\Delta\vartheta = \Delta\varphi = 28°$ in both angular directions, which justifies the use of a LFOV array.

The analysis is provided for subarrayed beamforming MMSE and CBF schemes and then the performance is compared to the benchmark beamforming design without subarraying. In order to have a fair comparison, the transmitted power in case of subarrayed BF has been divided by $(M_\text{H}M_\text{V})$, i.e., the maximum achievable subarray gain, so that the EIRP for both subarrayed and non-subarrayed cases shall be equivalent. Since a LFOV array has no steering capability at antenna-level, no hybrid beamforming is taken into account. We suppose Line

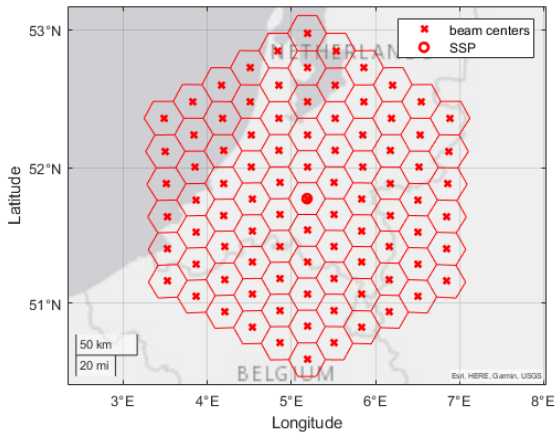

Fig. 3: Coverage area and generated beam lattice.

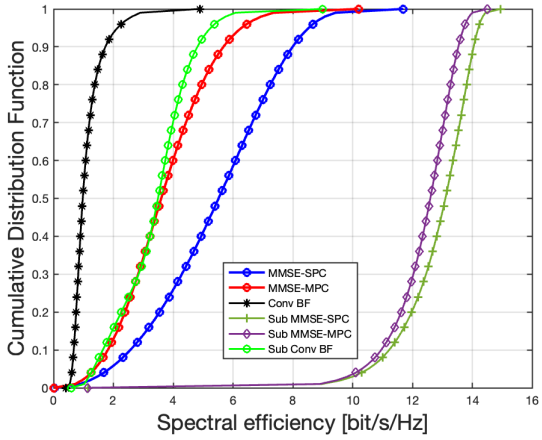

(a) Subarray 2×2

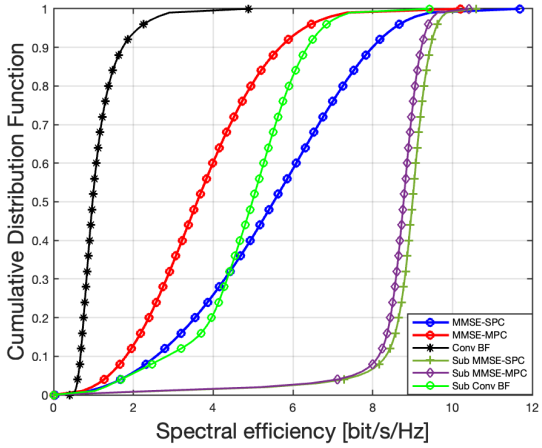

(b) Subarray 3×3

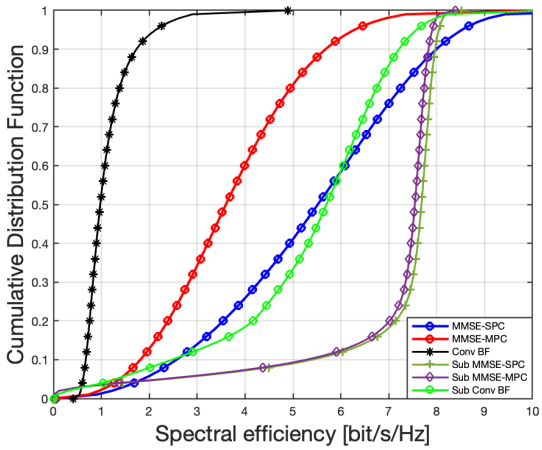

(c) Subarray 4×4

Fig. 4: CDF of users' spectral efficiency for VSATs considering different subarray configurations.

of Sight (LOS) propagation scenario in urban environment. According to 3GPP TR 38.821 [23], LOS scenario includes log-normal shadow fading, atmospheric loss, and scintillation. Fig. 4 shows the CDF of spectral efficiency of the users considering all the evaluated beamforming schemes with SPC and MPC normalization and three different subarray dimensions. It can be noted that the suggested BF configuration with 2×2 subarrays outperforms the BF design without subarraying for optimal MMSE followed by CBF. SPC performs better than MPC normalization since the latter does not exploit the whole available on-board power. In Fig. 4b, with subarray 3×3, we get a gain in the rate for MMSE-SPC in the order of 3.5 bit/sec/Hz, for MMSE-MPC in the order 5 bit/sec/Hz and for CBF in the order 3.5-4 bit/sec/Hz; whereas, in Fig. 4c, with subarray 4×4, we obtain a gain in the rate for MMSE-SPC in the order of 1.7-2 bit/sec/Hz, for MMSE-MPC in order 3-4 bit/sec/Hz and for CBF in the order 4-4.5 bit/sec/Hz. It is interesting to observe that analog CBF with 3×3 and 4×4 subarray configuration can clearly outperform digital MMSE with MPC normalization with no subarrays, while the performance of analog CBF with 4×4 subarray configuration and digital MMSE-SPC with no subarrays are very similar. Tab. II details the average values of the KPIs including SINR, Signal-to-Interference Ratio (SIR), SNR, INR and the rate of the considered BF schemes with different dimensions of subarrays compared to regular BF design without subarraying.The superiority of the subarrayed configuration over the non-subarrayed one for both MMSE and CBF is motivated by the fact the an LFOV array has highly improved directivity, i.e., it produces narrower beams over the service area. Consequently, such improved directivity enhances the interference rejection capability of the proposed beamforming techniques. Finally, by observing Figs. 4a, 4b, 4c, and Tab. II, it can be observed that the 2×2 is the best configuration for MMSE, while for larger subarray configurations, the loss of SNR due to the reduction in angular scanning range becomes the predominant factor; while for CBF, the 4×4 configurations exhibits the best performance as it shows the highest interference rejection capability (highest SIR and lowest INR).

TABLE II: Performance of BF with subarraying $M_{\text{H}} \times M_{\text{V}}$.

BF Scheme	KPIs				
	SINR [dB]	SIR [dB]	SNR [dB]	INR [dB]	Rate [bits/sec/Hz]
	Without Subarrays				
MMSE-SPC	15.93	18.09	25.21	7.12	5.40
MMSE-MPC	10.47	18.09	13.54	-4.55	3.69
CBF	0.35	0.35	47.75	47.40	1.11
	Subarray 2×2				
Sub MMSE-SPC	38.61	42.15	42.89	0.74	12.83
Sub MMSE-MPC	37.28	42.15	40.39	-1.76	12.38
Sub CBF	9.5	9.51	46.45	36.94	3.38
	Subarray 3×3				
Sub MMSE-SPC	26.38	39.71	26.95	-12.77	8.80
Sub MMSE-MPC	25.73	39.71	26.22	-13.49	8.59
Sub CBF	14.12	14.99	36.30	21.30	4.80
	Subarray 4×4				
Sub MMSE-SPC	20.56	37.69	20.84	-16.85	7.08
Sub MMSE-MPC	20.14	37.69	20.41	-17.28	6.95
Sub CBF	15.34	18.49	27.42	8.93	5.30

V. Conclusions

In this paper, we assessed subarrayed beamforming algorithms in LEO satellite systems. We assessed the performance of digital BF (MMSE) and analog BF as the benchmark algorithms dependent on CSI and non-CSI, respectively. Based on the numerical results, both digital and analog beamforming with subarraying proved to have significantly higher performance in terms of spectral efficiency w.r.t. a non-subarrayed architecture. The evaluation focused on the design of non-overlapped LFOV arrays with various dimensions in the configuration, and the beamforming has been implemented at subarray level only. In future works, we shall consider multiple satellites within a mega-constellation scenario that aims to achieve global coverage.

VI. Acknowledgments

This work has been funded by the 6G-NTN project, which received funding from the Smart Networks and Services Joint Undertaking (SNS JU) under the European Union's Horizon Europe research and innovation programme under Grant Agreement No 101096479. The views expressed are those of the authors and do not necessarily represent the project. The Commission is not liable for any use that may be made of any of the information contained therein.

References

[1] S. Liu et al., "LEO Satellite Constellations for 5G and Beyond: How Will They Reshape Vertical Domains?," *IEEE Communications Magazine*, vol. 59, no. 7, pp. 30-36, Jul. 2021.

[2] A. Guidotti et al., "The path to 5G-Advanced and 6G Non-Terrestrial Network systems," *2022 11th Advanced Satellite Multimedia Systems Conference and the 17th Signal Processing for Space Communications Workshop (ASMS/SPSC)*, 2022, pp. 1-8.

[3] V. Icolari, A. Guidotti, D. Tarchi, and A. Vanelli-Coralli, "An interference estimation technique for satellite cognitive radio systems", in *2015 IEEE International Conference on Communications (ICC)*, 2015, pp. 892–897.

[4] P.-D. Arapoglou et al., "Mimo over satellite: A review," *IEEE communications surveys & tutorials*, vol. 13, no. 1, pp. 27–51, 2010.

[5] L. You et al., "Massive MIMO transmission for LEO satellite communications," *IEEE Journal on Selected Areas in Communications*, vol. 38, no. 8, pp. 1851–1865, 2020.

[6] A. Guidotti and A. Vanelli-Coralli, "Clustering strategies for multicast Beamforming in multibeam satellite systems," *International Journal of Satellite Communications and Networking*, vol. 38, no. 2, pp. 85–104, 2020.

[7] A. Guidotti and A. Vanelli-Coralli, "Design trade-off analysis of Beamforming multi-beam satellite communication systems," in *2021 IEEE Aerospace Conference (50100)*, 2021, pp. 1–12.

[8] J. Palacios, N. Gonzalez-Prelcic, C. Mosquera, T. Shimizu, and C.-H. Wang, "A hybrid beamforming design for massive MIMO LEO satellite communications," *Frontiers in Space Technologies*, vol. 2, 2021.

[9] G. Caire et al., "Perspectives of adopting interference mitigation techniques in the context of broadband multimedia satellite systems," in *ICSSC 2005, 23rd AIAA International Communications Satellite Systems Conference*, 2005.

[10] P. Rocca, M. D'Urso and L. Poli, "Advanced Strategy for Large Antenna Array Design With Subarray-Only Amplitude and Phase Control," in *IEEE Antennas and Wireless Propagation Letters*, vol. 13, pp. 91-94, 2014.

[11] L. Manica, P. Rocca, and A. Massa, "Design of subarrayed linear and planar array antennas with SLL control based on an excitation matching approach," in *IEEE Trans. Antennas Propag.*, vol. 57, no. 6, pp. 1684–1691, Jun. 2009.

[12] R. J. Mailloux, S. G. Santarelli, T. M. Roberts, and D. Luu, "Irregular polyomino-shaped subarrays for space-based active arrays,", *International Journal of Antennas and Propagation*, vol. 2009, article ID 956524, 2009.

[13] T. Isernia, M.D'Urso and O. M. Bucci, "A simple idea for an effective sub-arraying of large planar sources," *IEEE Antennas Wireless Propag. Lett.*, vol. 8, pp. 169–172, 2009.

[14] J. Yang, X. Liu, Y. Tu and W. Li, "Robust Adaptive Beamforming Algorithm for Sparse Subarray Antenna Array Based on Hierarchical Weighting, *Micromachines*, 2022, 13, 859.

[15] Y. Aslan, J. Puskely, A. Roederer and A. Yarovoy, "Active Multiport Subarrays for 5G Communications," *2019 IEEE-APS Topical Conference on Antennas and Propagation in Wireless Communications (APWC)*, 2019, pp. 298-303.

[16] R. J. Mailloux, "Subarray technology for time delayed scanning arrays," in IEEE International Conference on COMCAS. IEEE, 2009, pp. 1–6.

[17] M. R. Dakkak, D. G. Riviello, A. Guidotti and A. Vanelli-Coralli, "Evaluation of MU-MIMO Digital Beamforming Algorithms in B5G/6G LEO Satellite Systems," *2022 11th Advanced Satellite Multimedia Systems Conference and the 17th Signal Processing for Space Communications Workshop (ASMS/SPSC)*, 2022, pp. 1-8.

[18] A. Guidotti, C. Amatetti, F. Arnal, B. Chamaillard and A. Vanelli-Coralli. "Location-assisted Beamforming in 5G LEO systems: architectures and performances", *2022 Joint European Conference on Networks and Communications & 6G Summit (EuCNC/6G Summit)*, Grenoble, France, 2022, pp. 154-159.

[19] D. G. Riviello, B. Ahmad, A. Guidotti and A. Vanelli-Coralli, "Joint Graph-based User Scheduling and Beamforming in LEO-MIMO Satellite Communication Systems," *2022 11th Advanced Satellite Multimedia Systems Conference and the 17th Signal Processing for Space Communications Workshop (ASMS/SPSC)*, 2022, pp. 1-8,

[20] ITU-R Radiocommunication Sector of ITU, "Modelling and simulation of IMT networks and systems for use in sharing and compatibility studies (M.2101-0)", Feb. 2017.

[21] G. Alfano, C.-F. Chiasserini, A. Nordio and D. G. Riviello, "A Random Matrix Model for mmWave MIMO Systems", *Acta Phys. Pol. B*, vol. 51, no. 7, pp. 1627-1640, 2020.

[22] Harry L. Van Trees, *Optimum Array Processing: Part IV of Detection, Estimation, and Modulation Theory*, John Wiley & Sons, 2004.

[23] 3GPP, "38.821 -Solutions for NR to support Non-Terrestrial Networks (NTN)", Jun. 2021.

[24] R. Muharar, J. Evans, "Downlink Beamforming with Transmit-side Channel Correlation: A Large System Analysis," *IEEE Int. Conf. on Commun. (ICC)*, Jun. 2011.

[25] P. Angeletti and R. De Gaudenzi, "A Pragmatic Approach to Massive MIMO for Broadband Communication Satellites," *IEEE Access, vol. 8, pp. 132 212–132 236*, 2020.